DRAFT VERSION FEBRUARY 23, 2015
Preprint typeset using LaTeX style emulateapj v. 08/13/06

ON COSMIC-RAY PRODUCTION EFFICIENCY AT SUPERNOVA REMNANT SHOCKS PROPAGATING INTO REALISTIC DIFFUSE INTERSTELLAR MEDIUM

JIRO SHIMODA[1], TSUYOSHI INOUE[2], YUTAKA OHIRA[1], RYO YAMAZAKI[1], AYA BAMBA[1], JACCO VINK[3]

Draft version February 23, 2015

ABSTRACT

Using three-dimensional magnetohydrodynamics simulations, we show that the efficiency of cosmic-ray (CR) production at supernova remnants (SNRs) is over-predicted if it could be estimated based on proper motion measurements of Hα filaments in combination with shock-jump conditions. Density fluctuations of upstream medium make shock waves rippled and oblique almost everywhere. The kinetic energy of the shock wave is transferred into that of downstream turbulence as well as thermal energy which is related to the shock velocity component normal to the shock surface. Our synthetic observation shows that the CR acceleration efficiency as estimated from a lower downstream plasma temperature, is overestimated by 10-40%, because rippled shock does not immediately dissipate all upstream kinetic energy.

Subject headings: acceleration of particles — ISM: supernova remnants — proper motions — shock waves — turbulence

1. INTRODUCTION

The energy density of Galactic cosmic rays (CRs) around the Earth is explained if 1–10 % of supernovae explosion energy are used to CR acceleration. The CR production efficiency at the supernova remnant (SNR) has been widely discussed, which seems to be ubiquitously so high that back reaction of CRs onto background shock structure is significant. One way to estimate the CR production efficiency is given by a combination of measurements of proper motion of shock front and temperature of shocked gas (e.g., Hughes et al. 2000; Tatischeff & Hernanz 2007; Helder et al. 2009; Morlino et al. 2013, 2014). The expansion speed of the SNR has been measured in various wavelength, from which the downstream temperature $T_{\rm proper}$ is predicted using Rankine-Hugoniot shock jump condition. If actual downstream temperature $T_{\rm down}$ can be independently measured, then the CR production efficiency η is given by

$$\eta = \frac{T_{\rm proper} - T_{\rm down}}{T_{\rm proper}} \quad , \tag{1}$$

where we assume the all missing thermal energy goes into CR production. Note that η can be related to β which was given by Equation (22) of Vink et al. (2010), as $\eta = 1 - \beta$. Observations of northeastern region of young SNR RCW86 gives us an example. The proper motion velocity of synchrotron X-ray filaments is measured as $\sim 6000 \pm 2800$ km s^{-1} (Helder et al. 2009), while those of Hα filaments range from 300 to 3000 km s^{-1} with the mean 1200 km s^{-1} (Helder et al. 2013). Let the expansion speed of the SNR be 3000 km s^{-1} so that X-ray and Hα observations are consistent with each other. If the proper motion velocity is equivalent to the shock velocity, the downstream proton temperature is predicted by Rankine-Hugoniot relation as $T_{\rm proper} = 17.6$ keV. This value is different from the direct measurement, $T_{\rm down} = 2.3 \pm 0.3$ keV, which is given by the line width of the broad component of Hα emission (Helder et al. 2009). Then, we obtain $\eta \approx 87$ %, which suggests extremely efficient CR acceleration. Even if the shock velocity is as low as 1200 km s^{-1}, the efficiency is 18 %.

In previous discussions, it was assumed that the shock was plane parallel — that is, the shock normal is parallel to the flow — and that the measured proper motion velocity was identical to the shock velocity. These assumptions would be suitable for spherical symmetric shock wave propagating into homogeneous medium. However, they may not be true for actual SNRs. The observed velocity of proper motion of Hα filaments is dispersed (e.g., Helder et al. 2013), which implies the shock propagation through inhomogeneous medium. At present, it is widely accepted that the interstellar medium is highly inhomogeneous (e.g., de Avillez & Breitschwerdt 2007), in particular, near the young SNRs (e.g., Fukui et al. 2003; Moriguchi et al. 2005). So far, we have investigated the effects of upstream inhomogeneity, and shown that various observational results can be explained (Inoue et al. 2009, 2010, 2012, 2013). Some predictions of magnetohydrodynamics (MHD) simulations, regarding magnetic field amplification due to turbulent dynamo downstream (Giacalone & Jokipii 2007; Inoue et al. 2009, 2012; Sano et al. 2012), have been observationally confirmed (Vink & Laming 2003; Bamba et al. 2003, 2005a,b; Yamazaki et al. 2004; Uchiyama et al. 2007; Sano et al. 2013, 2014). In this Letter, we will show that the above approximations may lead to overestimates of the CR production efficiency at SNRs. In order to study influence of upstream inhomogeneities, we perform three-dimensional (3D) MHD simulation of a shock wave propagating into inhomogeneous medium, and we simulate Hα filaments whose proper motion is synthetically measured.

2. SHOCK PROPAGATION THROUGH INHOMOGENEOUS ISM

Multi-dimensional MHD simulations of shock propagation through inhomogeneous diffuse ISM with Kolmogorov-like density power spectrum have shown that the shock front is rippled due to the fluctuating inertia of the preshock ISM (see Giacalone & Jokipii 2007 for 2D case and Inoue et al. 2013 for 3D case). Their results strongly suggest that SNR forward shock is locally oblique. For oblique shocks, downstream temperature is given by the velocity component normal to the

[1] Department of Physics and Mathematics, Aoyama-Gakuin University, Sagamihara, Kanagawa 252-5258, Japan; s-jiro@phys.aoyama.ac.jp
[2] National Astronomical Observatory of Japan, Mitaka, Tokyo 181-8588, Japan
[3] Astronomical Institute Anton Pannekoek/Gravitation and AstroParticle Physics Amsterdam (GRAPPA), University of Amsterdam, Science Park 904, 1098XH Amsterdam, The Netherlands

shock surface $V_{\rm n}$ (not shock velocity itself):

$$k_{\rm B}T_{\rm down} = \frac{3}{16}m_{\rm p}V_{\rm n}^2 \ , \quad (2)$$

where $k_{\rm B}$ and $m_{\rm p}$ are Boltzmann constant and proton mass, respectively. The velocity measured by proper motion is identical to the shock velocity component transverse to line of sight (LOS). Thus, when the shock front is rippled, the proper motion velocity, $V_{\rm proper}$, can be larger than $V_{\rm n}$. In Figure A1a, we illustrate the situation. The blue curved sheet represents part of the rippled shock front emitting Hα photons. As seen in the bottom of the figure, the limb brightening effect causes a peaked profile in surface brightness on the celestial sphere (Hester 1987). As the shock propagates, the peak of the brightness moves outwards (red sheet), which is observed as proper motion in the celestial sphere (magenta vector). Since $V_{\rm proper} \geq V_{\rm n}$, downstream temperature calculated based on the proper motion measurement can be overestimated, i.e., $T_{\rm proper} = 3m_{\rm p}V_{\rm proper}^2/(16k_{\rm B}) \geq T_{\rm down}$, so that η is apparently non-zero in spite of no CR acceleration. In the following, using the result of 3D MHD simulation of a shock propagation through an inhomogeneous medium performed by Inoue et al. (2013), we demonstrate that the above expectation is generally realized.

3. SET UP OF MHD SIMULATION

In this Letter, we use the data of the simulation performed by Inoue et al. (2013). Here we briefly summarize the setting of Inoue et al. (2013). They studied shock propagation into inhomogeneous medium that is parameterized by amplitude of density fluctuation $\Delta\rho/\langle\rho\rangle_0$ assuming the ideal MHD with adiabatic index $\gamma = 5/3$ and mean molecular weight of 1.27, where $\langle\rho\rangle_0$ is initial mean density and $\Delta\rho \equiv (\langle\rho^2\rangle - \langle\rho\rangle_0^2)^{1/2}$ is the dispersion. The fluctuations are given as a superposition of sinusoidal functions with various wave numbers ($2\pi/L_{\rm box} \leq |k| \leq 256\pi/L_{\rm box}$). The simulation is performed in a cubic numerical domain of the volume $L_{\rm box}^3 = (2\ {\rm pc})^3$ which is resolved by $(1024)^3$ unit cells. The power spectrum of the density fluctuations is given by the isotropic power law: $P_{\rm 1D}(k) \equiv \rho_k^2 k^2 \propto k^{-5/3}$ for the above range of k, where ρ_k is the Fourier component of the density. The above Kolmogorov spectrum is consistent with the observed Big-power-law-in-the-sky (Armstrong et al. 1995).

The initial mean number density, thermal pressure, and magnetic field strength are set to be $\langle n\rangle_0 = 0.5\ {\rm cm^{-3}}$, $P/k_{\rm B} = 4\times10^3\ {\rm K\ cm^{-3}}$, and $B_0 = 3.0\ \mu$G, respectively. These are the typical values in the diffuse ISM (Myers 1978; Beck 2000). Thus, the initial mean sound speed and Alfvén velocity are $\langle c_s\rangle = 9.3\ {\rm km\ s^{-1}}$, $\langle c_A\rangle = 8.2\ {\rm km\ s^{-1}}$, respectively. To induce a blast wave shock, we set a hot plasma of $p_{\rm h}/k_{\rm B} = 2\times10^8\ {\rm K\ cm^{-3}}$, $n_{\rm h} = 0.05\ {\rm cm^{-3}}$, and $B_{\rm h} = 3.0\ \mu$G at the $x = 0$ boundary plane. The resulting mean propagation speed of the shock is $1800\ {\rm km\ s^{-1}}$ that is suitable for studying young SNR, although local shock velocity has large dispersion due to the shock rippling.

In this Letter, we use data of the simulation for $\Delta\rho/\langle\rho\rangle_0 = 0.3$, which can be regarded as a typical ISM model. The reason is as follows: if we suppose the turbulence in the ISM driven by supernovae, the driving scale of the turbulence and the degree of density fluctuation at the driving scale would be given as $L_{\rm inj} \sim 100$ pc and $\Delta\rho|_{L_{\rm inj}}/\langle\rho\rangle_0 \sim 1$, respectively (e.g., de Avillez & Breitschwerdt 2007). In that case, the degree of small-scale density fluctuations due to cascade of the turbulence at the scale $L_{\rm box} = 2$ pc is estimated as $\Delta\rho|_{L_{\rm inj}}/\langle\rho\rangle_0 \simeq (L_{\rm box}/L_{\rm inj})^{1/3} \sim 0.3$.

4. RESULTS OF MHD SIMULATION AND SYNTHETIC OBSERVATIONS

In this section, we show simulation results. The top panel of Figure A2 represents the two-dimensional slice of the proton temperature (*upper half*) and the number density (*lower half*) at $t_{\rm obs} = 700$ yr and $z = 0$ pc plane. The proton temperature is estimated from $T_{\rm p} = P/(\rho k_{\rm B})$, where P and ρ are the pressure and density. From Figure A2, we can recognize that shock waves propagate into realistic ISM with various angles and velocities. As a result, the temperature distribution is inhomogeneous (see, the black curve of Figure A3). In this inhomogeneous system, it may be that the relation between the proper motion velocity of Hα and the downstream temperature does not satisfy Rankine-Hugoniot relations.

In order to estimate the deviation from Rankine-Hugoniot relations, we calculate the proper motion of Hα emission during 10 years (from $t_{\rm obs} = 700$ to 710 yr). The Hα emission observed from SNRs sometimes has narrow and broad components. The former is a characteristic of the cold interstellar medium, which arises from direct excitation of the neutral hydrogen atoms crossing the shock surface. The latter is a characteristic of the thermal broadening of the shocked protons, which arises from hot hydrogen atoms generated by charge exchange reaction between cold neutrals and the shocked protons. In this Letter, we calculate only the narrow component of Hα emission from our MHD simulation because the broad component of Hα is not necessarily observed from SNRs. We consider hydrogen atoms, electrons and protons as particles. Results of our MHD simulation are valid as long as the ionization fraction of the upstream gas is sufficiently high because our MHD simulation does not take into account ionization of neutral hydrogen atoms. Recent studies have shown that ionization of neutral hydrogen atoms changes collisionless shock structures (Ohira et al. 2009; Ohira & Takahara 2010; Ohira 2012, 2013, 2014; Blasi et al. 2012). Therefore, we consider a highly ionized upstream gas in this letter because effects of ionization can be neglected.

According to Heng & McCray (2007), the rate (in units of $\rm s^{-1}$) that hydrogen atoms (denoted H) will have a reaction X (X = E, I, and CE for excitaion, ionization, and charge exchange) with particles type of s (s = e and p for electrons and protons, respectively) is given by

$$R_{X,s} = n_s \int d^3\vec{v}_{\rm H} \int d^3\vec{v}_s f_{\rm H}(\vec{v}_{\rm H}) f(\vec{v}_s) \Delta v_s \sigma_{X,s}(\Delta v_s) \ , \quad (3)$$

where n_s, $\vec{v}_s$ and f_s are the number density, the velocity, and the distribution function for particle s, respectively. Velocity and the distribution function of hydrogen atoms are described as $\vec{v}_{\rm H}$ and $f_{\rm H}$, respectively. The relative velocity between neutral hydrogen atoms and particle s is denoted by $\Delta v_s = |\vec{v}_{\rm H} - \vec{v}_s|$. We assume that distribution functions for each particle are represented by

$$f_{\rm H} = \delta(\vec{v}_{\rm H}) \ , \quad (4)$$

$$f_s = \left(\frac{m_s}{2\pi k_{\rm B}T_s(\vec{r})}\right)^{3/2} \exp\left(-\frac{m_s v_s^2(\vec{r})}{2k_{\rm B}T_s(\vec{r})}\right) \ , \quad (5)$$

where $v_s(\vec{r}) = |\vec{v}_s - \vec{u}(\vec{r})|$, and $\vec{u}(\vec{r})$ is the downstream fluid velocity. We regard the distribution function of hydrogen atoms as Dirac delta function because we consider only the narrow

component. In addition, we assume that distribution functions of protons and electrons are Maxwellian with $T_{\rm p} = P/(\rho k_{\rm B})$ and $T_{\rm e} = 0.01 T_{\rm p}$, respectively (Ohira & Takahara 2007, 2008; Rakowski et al. 2008). In order to calculate equation (3), we use our MHD simulation data for $u(\vec{r})$, $T_{\rm p}(\vec{r})$, and $n_s(\vec{r})$, as well as data of Janev & Smith (1993) for cross sections. Calculating the excitation rate, $R_{\rm E} = R_{\rm E,p} + R_{\rm E,e}$, for each cell of our MHD simulation and integrating $n_{\rm H}(\vec{r})R_{\rm E}(\vec{r})$ along LOS (z-axis), we obtain the surface emissivity of the Hα emission,

$$S(x,y) = \int n_{\rm H}(\vec{r}) R_{\rm E}(\vec{r}) dz \ , \tag{6}$$

where we consider only direct excitation from the ground state to $n = 3$ level. Neutral hydrogen atoms are ionized in the downstream region. The density of neutral hydrogen atoms in the downstream region is given by

$$n_{\rm H}(\vec{r}) = n_{\rm H,0}(\vec{r}) \exp\left[-R_{\rm I}(\vec{r})(t_{\rm obs} - t_{\rm sh}(\vec{r}))\right] \ , \tag{7}$$

where $R_{\rm I}(\vec{r}) = R_{\rm I,p}(\vec{r}) + R_{\rm CE,p}(\vec{r}) + R_{\rm I,e}(\vec{r})$, and $t_{\rm sh}(\vec{r})$ is the time when the shock wave passes though the point $\vec{r}$. For the initial hydrogen density, $n_{\rm H}$, we assume that the initial ionization fraction of the ISM is uniform. The bottom panel of Figure A2 is the Hα image obtained from equations (3)–(7).

As shown in the bottom panel of Figure A2, we select 16 regions which contains clear filamentary structure of Hα to measure proper motion. We extract surface brightness profile from these regions and analyze their proper motions by the same way as Helder et al. (2013). To measure the proper motion, we shift the normalized profiles over one another in steps of 1 bins, calculating the χ^2 values for each shift. Length of 1 bin is taken as 1.9×10^{15}cm, which is comparable to the angular resolution of optical instrument for the typical distance to the source of a few kpc. The best-fitting shift is determined by fitting a parabola to the three χ^2 values surrounding the minimal χ^2. We estimate the 1-σ uncertainties on the best-fitted proper motion, which correspond to $\Delta\chi^2 = 1$. Then, the best fitted proper motion velocity $V_{\rm proper}$ is related to $T_{\rm proper}$ as $T_{\rm proper} = 3 m_{\rm p} V_{\rm proper}^2 / 16 k_{\rm B}$, which is the same way as in the previous actual observational studies.

In order to evaluate η from equation (1), we calculate the downstream proton temperature $T_{\rm down}$ in two ways. First, we take $T_{\rm down}$ as a mean of downstream temperatures of fluid cells just behind the shock surface on the LOS crossing the Hα filament (Case 1). As a typical example, we show in Figure A3 the distributions of proton temperature $T_{\rm down}$ of the fluid cell just behind the shock surface; the black curve is for the whole shock surface, while the blue is for the surface on the LOS crossing the Hα filament of Region 3. Note that the proper motion velocity of Region 3 corresponds to the mean of our 16 regions (see Table A1). The vertical magenta line represents $T_{\rm proper}$ for Region 3 with magenta belt showing associated error. The value of $T_{\rm proper}$ is higher than the mean of $T_{\rm down}$. We calculate, from equation (1), apparent CR production efficiency as $\eta \sim 0.3 \pm 0.1$.

Next, we consider similar situation to actual observations where downstream temperature $T_{\rm down}$ is estimated from the line width of the broad Hα component (Case 2). It is hard to calculate exactly the broad emission component in our model. Instead, we perform simple, approximate calculation. We obtain $T_{\rm down}$ from the FWHM of the sum of shifted Maxwellian weighted by the brightness of the broad Hα component, $n_{\rm H,0}(\vec{r})\xi_{\rm CE}(\vec{r})$, of the fluid cell at $\vec{r}$ just behind the shock surface on the LOS crossing the Hα filament, where $\xi_{\rm CE}(\vec{r}) = R_{\rm CE,p}(\vec{r})[R_{\rm I,p}(\vec{r}) + R_{\rm I,e}(\vec{r})]^{-1}$. Then, we find η becomes slightly larger than those for Case 1 (Table A1). This is because the hot hydrogen atom emitting the broad Hα component is generated by charge exchange reaction, whose cross-section decreases rapidly if relative velocity is higher than ≈ 2000 km s^{-1}. Thus, the observed downstream temperature may be biased against the particular temperature. This effect has already been investigated for one-dimensional shock wave by detailed analysis of Hα emission (van Adelsberg et al. 2008). Since rippled shock front generates dispersion of downstream fluid velocity, one might consider that the line width is spread by downstream bulk motion. If this Doppler effect were significant, measured $T_{\rm down}$ would tend to be higher than the actual downstream proton temperature, resulting lower η. However, this is not the case for our present synthetic observation. It is known for oblique shocks that in the upstream rest frame, the downstream fluid velocity $\vec{u}$ is parallel to the shock normal (Figure A1b). Hence, if the rippled shock front is viewed from nearly edge-on as in the present case, the Doppler broadening is not so significant.

Table A1 shows the measured proper motion velocity and apparent CR production efficiency η for the 16 regions. As expected in section 2, $T_{\rm proper}$ is higher than $T_{\rm down}$, and the efficiency η is positive (see also Figure 4), even though our simulation do not involves the effects of comic-ray acceleration.

5. DISCUSSION

We have shown that the CR production efficiency η seems to be overestimated at the shock wave of SNRs propagating into realistic ISM if the postshock temperature $T_{\rm proper}$ is estimated from the proper motion of Hα filaments in combination with Rankine-Hugoniot relation for plane-parallel shock. It may not be suitable assumptions for actual SNR shocks that the shock wave is plane parallel and that the measured proper motion velocity is equivalent to the shock velocity. Density fluctuations of realistic ISM make the rippled, locally oblique shock front almost everywhere. For the oblique shocks, the postshock temperature is given not by shock velocity itself but by the velocity component normal to the shock surface $V_{\rm n}$ as shown by equation (2). Because proper motion measurements give us velocity component transverse to LOS (see Figure A1), the predicted postshock temperature $T_{\rm proper}$ given by Rankine-Hugoniot relation with the assumption of plane parallel shock is larger than actual downstream temperature $T_{\rm down}$. Therefore, we claim that the CR production efficiency η has some uncertainty, and it can be positive (up to 0.4 in our case) in spite of no CR acceleration.

As shown in the Appendix, a simple analytical argument gives the upper and lower bounds of η as

$$\left(\frac{\Delta\rho}{\langle\rho\rangle_0}\right)^2 \lesssim \eta \lesssim 2\frac{\Delta\rho}{\langle\rho\rangle_0} \ , \tag{8}$$

where $\Delta\rho/\langle\rho\rangle_0$ is the upstream density fluctuation at the scale $L_{\rm box} = 2$ pc. Since we have set $\Delta\rho/\langle\rho\rangle_0 = 0.3$ in our present simulation study, this analytical formula is roughly consistent with our numerical result. RCW 86 is likely a SNR expanding in the windblown bubble (Vink et al. 1997, 2006) and a part of the shock collided with dense clumps and/or cavity wall very recently (Yamaguchi et al. 2008), so that we expect larger value of $\Delta\rho/\langle\rho\rangle_0$ than that of ISM. If the CR acceleration is inefficient so that nonlinear effect can be neglected, then we expect $\Delta\rho/\langle\rho\rangle_0 \approx 0.4$ in order to explain the observational result $\eta = 0.2$–0.9 (see section 1). On the other hand, shock deformation in ~ 10 pc scale may be smaller for SNRs such

as SN 1006, Tycho's remnant, and SNR 0509–67.5, which are embedded in ISM with smaller $\Delta\rho/\langle\rho\rangle_0$ than RCW 86. Global Hα image of SN 1006, whose radius is about 10 pc, looks like a circular ring except for the northwestern region, while smaller-scale ($\lesssim$ a few pc) rippling can also be seen (Raymond et al. 2007; Winkler et al. 2014). Tycho's remnant has radius of about 3 pc, and its whole Hα shape is no longer circular (Raymond et al. 2010). Indeed, several observational results have indicated inhomogeneity of ambient medium around SN 1006 (Dubner et al. 2002; Raymond et al. 2007; Miceli et al. 2014) and Tycho's remnant (Ishihara et al. 2010; Reynoso et al. 1991). SNR 0509–67.5 is also round in shape with a radius of 3.6 pc, however, southwest part of the remnant is rippled and has many Hα filaments (see e.g., Fig. 1 of Helder et al. 2010). These observational results on Hα morphology in a few pc or smaller scale are consistent with our model with typical ISM density fluctuation. Therefore, we should still pay attention to the effect of upstream inhomogeneity when the CR acceleration efficiency is discussed in these remnants. In order to reproduce the morphology of the whole remnant and smaller scale structure simultaneously, larger scale simulation is required keeping the same spatial resolution as the present study, which is currently difficult due to the limitation of computer resources and remains a future work.

At oblique shocks, upstream velocity component parallel to the shock front is not dissipated across the shock. For the case of edge-on view of the rippled shock, such component mainly turns to be transverse to LOS in the downstream region (see Figure 1a), so that it becomes unseen, missing component — it does not even contribute to the width of the broad Hα line. In the previous observational arguments, the missing energy was attributed to CR acceleration. In the present case, post-shock fluid stream lines become "turbulence" after the crossing time of the shock rippling scale (the driving scale of "turbulence"). Note that this driving scale ~ 0.1 pc (Inoue et al. 2013) is much larger than the typical width of emission region, indicating that turbulent line broadening cannot be measured by Hα emissions. Since the downstream turbulence is created by the effect of the rippled shock wave (Giacalone & Jokipii 2007), the induction of the turbulence can be understood as a consequence of Crocco's theorem in hydrodynamics. The strength of the induced turbulence depends on the degree of the density inhomogeneity in the preshock medium. In Inoue et al. (2013), we found that the velocity dispersion of turbulence can be well described by a formula obtained from modified grow velocity of the Richtmyer-Meshkov instability as a function of the upstream density dispersion.

One can also find from synthetic Hα image (bottom panel of Figure A2), that regions 1–6 precede regions 9–12, so that one might think that the proper motion velocities of regions 1–6 are higher than those of regions 9–12. However, this is not true (see Table 1). We find outermost parts of the Hα filament does not always have the fastest shock velocity nor the highest downstream temperature. This is because the shock front has effective surface tension and is stable with respect to the rippling deformations. Thus, even though some regions of the shock front is decelerated (accelerated) due to passage of the dense (thin) region, it will be accelerated (decelerated) once the dense (thin) region passes into the downstream region.

In the present analysis, we have seen $\eta \geq 0$ (that is, $T_{\rm proper} > T_{\rm down}$) for all 16 regions, which implies the proper motion velocity $V_{\rm proper}$ is larger than the velocity component normal to shock surface $V_{\rm n}$. We have set our LOS orthogonal to the global direction of the shock propagation. However, when the shock wave propagates nearly toward us (along the LOS), $V_{\rm proper}$ can be smaller than $V_{\rm n}$. For example, Salvesen et al. (2009) measured the proper motion velocity of Hα filaments of Cygnus Loop and simultaneously derived downstream gas temperature from thermal X-ray spectrum there. Then, they obtained the fraction of the CR pressure $P_{\rm CR}$ to the thermal gas pressure $P_{\rm G}$ in the downstream region. According to their analysis, many Hα filaments have $P_{\rm CR}/P_{\rm G} \leq 0$. Since they assumed a strong shock with the compression ratio of 4, the adiabatic index of 5/3, and the temperature equilibrium $T_e = T_i = T_{\rm down}$, the ratio $P_{\rm CR}/P_{\rm G}$ is related to η as

$$\frac{P_{\rm CR}}{P_{\rm G}} = \frac{\eta}{1-\eta} \quad . \tag{9}$$

Here T_e and T_i are downstream electron and ion temperatures, respectively. Since $\eta > 1$ is unphysical, $P_{\rm CR}/P_{\rm G} < 0$ means $\eta < 0$, that is, $T_{\rm proper} < T_{\rm down}$. Therefore, the observational result on Cygnus Loop might be explained by our model. Moreover, it is suggested that the proper motion velocity is underestimated due to the shock obliqueness.

We would like to thank the referee for useful comments and suggestions. Numerical computations were carried out on XC30 system at the Center for Computational Astrophysics (CfCA) of National Astronomical Observatory of Japan and K computer at the RIKEN Advanced Institute for Computational Science (No. hp120087). This work is supported by Grant-in-aids from the Ministry of Education, Culture, Sports, Science, and Technology (MEXT) of Japan, No. 23740154 (T. I.) and No. 248344 (Y. O.), No. 22684012 (A.B.). T. I. and R. Y. deeply appreciate Research Institute, Aoyama-Gakuin University for helping our research by the fund. R. Y. also thank ISSI (Bern) for support of the team "Physics of the Injection of Particle Acceleration at Astrophysical, Heliospheric, and Laboratory Collisionless Shocks".

APPENDIX

ANALYTICAL ESTIMATE OF η

We present a simple analytical argument which relates η to the upstream density fluctuation. We simplify the upstream medium as a mixture of two components: overdense clumps with density $\langle\rho\rangle_0 + \Delta\rho$ and underdense gas with density $\langle\rho\rangle_0 - \Delta\rho$. Characteristic size of the clumps λ is the same as their separation. In the present case, λ is on the order of $L_{\rm box} = 2$ pc. Initially planar shock surface collides with the clumps. Its propagation speed in the clumps V_+ is slower than that in the underdense gas V_-, so that the shock surface is deformed. Assuming momentum conservation, these are related as

$$(\langle\rho\rangle_0 + \Delta\rho)V_+^2 \approx (\langle\rho\rangle_0 - \Delta\rho)V_-^2 \quad . \tag{A1}$$

Then, we find $V_+/V_- \approx 1 - \Delta\rho/\langle\rho\rangle_0$ for small $\Delta\rho/\langle\rho\rangle_0$. As the shock front goes ahead a distance λ in the underdense gas, the shock surface in the clumps is left a distance $\delta = \lambda - (\lambda/V_-)V_+$ behind the preceding surface in the underdense gas. Therefore,

TABLE A1
CALCULATION RESULTS FOR SELECTED 16 REGIONS

Region	$V_{\rm proper}$ [10^8cm s^{-1}]	$T_{\rm proper}$ [keV]	Case 1 $T_{\rm down}$ [keV]	Case 1 η	Case 2 $T_{\rm down}$ [keV]	Case 2 η
1	1.8±0.1	6.0±0.5	5.7	0.06±0.07	5.5	0.08±0.07
2	1.8±0.0	6.6±0.3	6.0	0.09±0.04	5.7	0.14±0.04
3	1.7±0.1	5.8±0.8	4.2	0.27±0.09	3.9	0.33±0.08
4	1.4±0.1	3.7±0.4	3.0	0.19±0.08	2.9	0.22±0.07
5	1.4±0.1	3.7±0.4	2.6	0.28±0.08	2.6	0.29±0.08
6	1.4±0.0	4.0±0.2	2.9	0.28±0.04	2.8	0.30±0.03
7	1.4±0.1	3.9±0.6	3.3	0.20±0.10	3.1	0.20±0.11
8	1.7±0.1	5.4±0.6	4.1	0.24±0.08	3.9	0.28±0.08
9	2.0±0.1	7.5±0.9	5.1	0.32±0.07	4.9	0.34±0.07
10	2.1±0.0	8.2±0.2	5.5	0.33±0.02	5.2	0.36±0.02
11	2.0±0.0	8.2±0.3	5.2	0.37±0.02	5.0	0.39±0.02
12	1.9±0.1	7.2±0.6	4.3	0.40±0.05	4.3	0.41±0.05
13	1.6±0.1	5.2±0.5	3.5	0.33±0.06	3.4	0.35±0.06
14	1.6±0.1	5.0±0.6	4.3	0.10±0.10	3.9	0.22±0.09
15	1.4±0.1	4.0±0.4	2.9	0.27±0.07	2.9	0.29±0.07
16	2.0±0.0	8.2±0.1	7.2	0.11±0.01	7.7	0.06±0.01
Mean/std. dev.	1.7/0.24	5.8/1.6	4.4/1.3	0.24/0.10	4.2/1.3	0.27/0.10

one derives the deformation angle θ, which is an angle between shock velocity $\vec{V}_{\rm sh}$ and the shock normal (see the right panel of Figure 1), as $\theta \approx \delta/\lambda \approx \Delta\rho/\langle\rho\rangle_0$.

Downstream temperature $T_{\rm down}$ is predominantly determined by the overdense clump, that is, Equation (2) with $V_{\rm n} = V_+\cos\theta$. For our present geometry, in which shock surface are viewed from nearly edge-on, proper motion velocity $V_{\rm proper}$ is roughly equal to the shock velocity $V_{\rm sh}$. If we observe the proper motion velocity of the shock surface propagating into the overdense clump, then $V_{\rm proper} \approx V_+$, while $V_{\rm proper} \approx V_-$ for the shock propagation into the underdense gas. Hence, we find $\eta = 1-\cos^2\theta \approx (\Delta\rho/\langle\rho\rangle_0)^2$ for the former case, while $\eta = 1-(V_+/V_-)^2\cos^2\theta \approx 2\Delta\rho/\langle\rho\rangle_0$ for the latter case. In more complicated case of our present simulation study, we expect $V_+ \lesssim V_{\rm sh} \lesssim V_-$ and these values of η may give lower and upper bounds, so that $(\Delta\rho/\langle\rho\rangle_0)^2 \lesssim \eta \lesssim 2\Delta\rho/\langle\rho\rangle_0$.

REFERENCES

Armstrong, J. W., Rickett, B. J., & Spangler, S. R. 1995, ApJ, 443, 209
Bamba, A., et al. 2003, ApJ, 589, 827
Bamba, A., et al. 2005a, ApJ, 621, 793
Bamba, A., Yamazaki, R., & Hiraga, J. S. 2005b, ApJ, 632, 294
Beck, R. 2000, Space Sci. Rev., 99, 243
Blasi, P., Morlino, G., Bandiera R., Amato, E., & Caprioli, D., 2012, ApJ, 755, 121
de Avillez, M. A., & Breitschwerdt, D. 2007, ApJ, 665, 35
Dubner, G. M., Giacani, E. B., Goss W. M., et al. 2002, A&A, 387, 1047
Fukui, Y. et al. 2003, PASJ, 55, L61
Giacalone, J., & Jokipii, J. R. 2007, ApJ, 663, 41
Helder, E. A., Vink, J., Bamba, et al. 2013, MNRAS, 435, 910
Helder, E. A., Kosenko, D. & Vink, J. 2010, ApJ, 719, L140
Helder, E.A., Vink, J., Bassa, C. G. et al. 2009, Sci, 325, 719
Heng, K., & McCray, R. 2007, ApJ, 654, 923
Hester, J. J. 1987, ApJ, 314, 187
Hughes, J. P., Rakowski, C. E., & Decourchelle, A. 2000, ApJ, 543, L61
Inoue, T., Yamazaki, R., & Inutsuka, S. 2009, ApJ, 695, 825
Inoue, T., Yamazaki, R., & Inutsuka, S. 2010, ApJ, 723, L108
Inoue, T., Yamazaki, R., Inutsuka, S., & Fukui, Y. 2012, ApJ, 744, 71
Inoue, T., Shimoda, J., Ohira, Y., & Yamazaki, R. 2013, ApJ, 772, L20
Ishihara, D., Kaneda, H., Fukuzawa, A. et al. 2010 A&A, 521, L61
Janev, R. K., & Smith, J. J. 1993, Cross Sections for Collision Processes of Hydrogen Atoms with Electrons, Protons and Multiply Charged Ions (Vienna: Int. At. Energy Agency)
Miceli, M., Acero, F., Dubner, G. et al. 2014, ApJ, 782, L33
Morlino, G., Blasi, P., Bandiera, R., & Amato, E. 2014 A&A 562, A141
Morlino, G., Blasi, P., Bandiera, R., & Amato, E. 2013 A&A 557, A142
Moriguchi, Y. et al. 2005, ApJ, 631, 947
Myers, P. C. 1978, ApJ, 225, 380
Ohira, Y., & Takahara, F., 2007, ApJ, 661, L171
Ohira, Y., & Takahara, F., 2008, ApJ, 688, 320
Ohira, Y., Terasawa, T., & Takahara, F., 2009, ApJ, 703, L59
Ohira, Y., & Takahara, F., 2010, ApJ, 721, L43
Ohira, Y., 2012, ApJ, 758, 97
Ohira, Y., 2013, Phys. Rev. Lett., 111, 245002
Ohira, Y., 2014, MNRAS, 440, 514
Rakowski, C. E., Laming, J. M., & Ghavamian, P., 2008, ApJ, 684, 348
Raymond, J.C., Korreck, K.E., Sedlacek, Q.C., Blair, W. P. et al., 2007 ApJ, 659, 1257
Raymond, J.C., Winkler, P. F., Blair, W. P. et al., 2010 ApJ, 712, 901
Reynoso, E. M., Velázquez, P. F., Dubner, G. M., & Goss, W. M. 1991, AJ, 117, 1827
Sano, T., Nishihara, K., Matsuoka, C. & Inoue, T. 2012, ApJ, 758, 126
Sano, H., Tanaka, T., Torii, K., Fukuda, T. et al. 2013, ApJ, 778, L59
Sano, H., Fukuda, T., Yoshiike, S., Sato, J. et al. 2014, arXiv:1401.7418
Salvesen, G., Raymond, J., C., & Edgar, R., E. 2009 ApJ, 702, 327
Tatischeff, V. & Hernanz, M. 2007, ApJ, 663, L101
Uchiyama, Y. et al. 2007, Nature, 449, 576
van Adelsberg, M. et al. 2008, ApJ, 689, 1089
Vink, J. et al. 1997, A&A, 328, 628
Vink, J. et al. 2006, ApJ, 648, L33
Vink, J., & Laming, J. M. 2003, ApJ, 584, 758
Vink, J., Yamazaki, R., Helder, E.A. et al. 2010, ApJ, 722, 1727
Winkler, P. F. et al. 2014, ApJ, 781, 65
Yamaguchi, H., Koyama, K., Nakajima, H. et al. 2008, PASJ, 60, S123
Yamazaki, R., Yoshida, T., Terasawa, T. et al. 2004, A&A, 416, 595

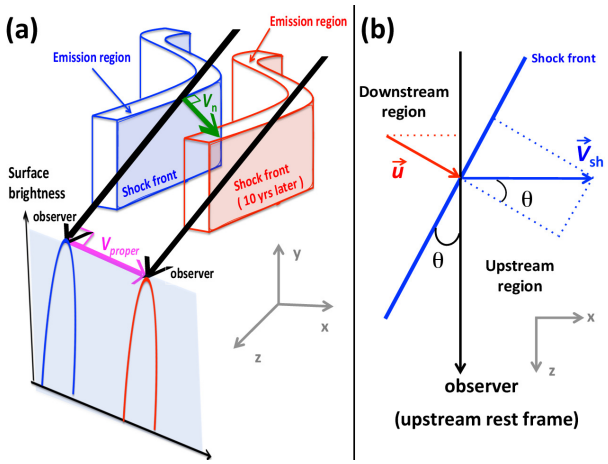

FIG. A1.— (a) Left panel shows the relation between proper motion velocity and the velocity component normal to shock surface for rippled shock. The curved blue sheet represents a part of rippled shock front and emission region of Hα. The curved red sheet also represents those after a short-time propagation. Thick black arrows show LOSs. Limb brightening effect causes a peaked profile in surface brightness as shown in the inner panel. The magenta and green vectors represent observed proper motion velocity $V_{\rm proper}$ and the velocity component normal to the shock surface $V_{\rm n}$, respectively. One can see that $V_{\rm proper}$ is generally larger than $V_{\rm n}$. (b) Right panel shows enlarged view of the local oblique shock. The blue line represents the shock front that propagates along the x-axis, and the LOS direction (black arrow) is taken along z-axis. In the upstream rest frame, the downstream fluid velocity $\vec{u}$ is definitively parallel to the shock normal. The z-component of $\vec{u}$ causes the Doppler shift of broad Hα line emission from this region.

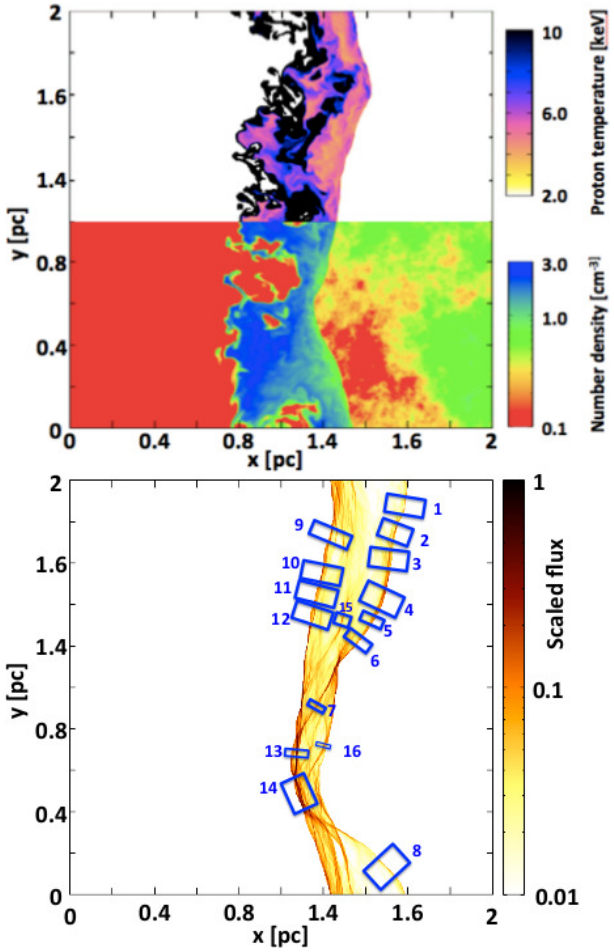

FIG. A2.— (top panel) Two-dimensional slice of the proton temperature (*upper half*) and the number density (*lower half*) at $t_{\rm obs}$ = 700 yr and z = 0 pc plane. (bottom panel) Simulated Hα image. We set the LOS along z-axis. Color represents scaled flux of Hα. We selected 16 local regions (*blue box*), in which proper motion of Hα filament is measured to predict downstream proton temperature.

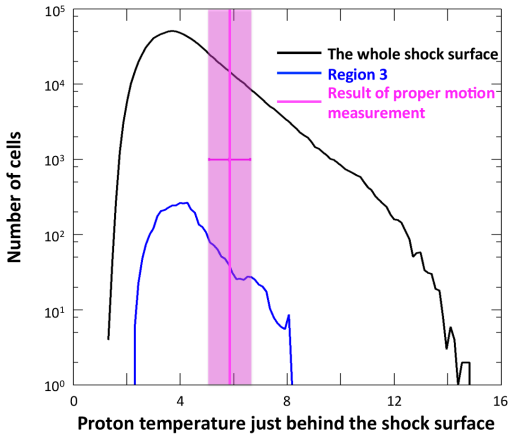

FIG. A3.— Distributions of proton temperature of the fluid cell just behind the shock surface. The black curve is for the whole shock surface, while the blue is for the surface on the LOS crossing the Hα filament of Region 3. The vertical magenta line represents downstream proton temperature, $T_{\rm proper}$, which is inferred from the best fitted proper motion velocity, with magenta belt showing associated error.